Title
Electrophysiology and Arrhythmogenesis in the Human Right Ventricular Outflow Tract

Journal
Circulation Arrhythmia and Electrophysiology, 15(3)

ISSN
1941-3149

Authors
Aras, Kedar
Gams, Anna
Faye, Ndeye Rokhaya
et al.

Publication Date
2022-03-01

DOI
10.1161/circep.121.010630

Peer reviewed

HHS Public Access

Author manuscript

Circ Arrhythm Electrophysiol. Author manuscript; available in PMC 2023 March 03.

Published in final edited form as:

Circ Arrhythm Electrophysiol. 2022 March ; 15(3): e010630. doi:10.1161/CIRCEP.121.010630.

Electrophysiology and Arrhythmogenesis in the Human Right Ventricle Outflow Tract

Kedar Aras, PhD[1,8], **Anna Gams, BS**[1], **Rokhaya Faye, PhD**[1,2], **Jaclyn Brennan, PhD**[1], **Katherine Goldrick, BS**[1], **Jinghua Li, PhD**[3,8], **Yishan Zhong, PhD**[4], **Chia-Han Chiang, PhD**[5], **Elizabeth H. Smith, BS**[6], **Megan D. Poston, BS**[6], **Jacqueline Chivers, BS**[6], **Peter Hanna, MD, PhD**[7], **Shumpei Mori, MD, PhD**[7], **Olujimi A. Ajijola, MD, PhD**[7], **Kalyanam Shivkumar, MD, PhD**[7], **Donald B. Hoover, PhD**[6], **Jonathan Viventi, PhD**[5], **John A. Rogers, PhD**[3], **Olivier Bernus, PhD**[2], **Igor R. Efimov, PhD**[1]

[1]Department of Biomedical Engineering, the George Washington University, Washington, DC

[2]LIRYC Institute, Bordeaux University, France

[3]Department of Biomedical Engineering, Northwestern University, Evanston, IL

[4]Department of Electrical and Computer Engineering, University of Illinois at Urbana-Champaign, IL

[5]Department of Biomedical Engineering, Duke University, Durham, NC

[6]Department of Biomedical Sciences, East Tennessee State University, Johnson City, TN

[7]UCLA Cardiac Arrhythmia Center and Neurocardiology Research Program of Excellence, University of California Los Angeles, Los Angeles, CA

[8]Department of Materials Science and Engineering, Ohio State University, Columbus, OH

Abstract

Background: Right ventricular outflow tract (RVOT) is a common source of ventricular tachycardia, which often requires ablation. However, the mechanisms underlying the RVOT's unique arrhythmia susceptibility remain poorly understood due to lack of detailed electrophysiological and molecular studies of the human RVOT.

Methods: We conducted optical mapping studies in 16 non-diseased donor human RVOT preparations subjected to pharmacologically induced adrenergic and cholinergic stimulation to evaluate susceptibility to arrhythmias and characterize arrhythmia dynamics.

Results: We found that under control conditions, RVOT has shorter action potential duration (APD80) relative to the right ventricular apical region (RVAR). Treatment with isoproterenol (100nM) shortened APD80 and increased incidence of premature ventricular contractions (PVCs) ($p=0.003$), whereas acetylcholine (100μM) stimulation alone had no effect on APD80 or PVCs.

Corresponding Author(s): Igor Efimov, efimov@gwu.edu phone: 202-294-8182, and Kedar Aras, kedar_aras@gwu.edu, phone: 269-519-3818, address: Department of Biomedical Engineering, the George Washington University, Science and Engineering Hall, Washington, DC, 20052, USA.

Disclosures: None

However, acetylcholine treatment after isoproterenol stimulation, reduced the incidence of PVCs (p=0.034) and partially reversed APD80 shortening (p=0.029). Immunolabeling of RVOT (n=4) confirmed the presence of cholinergic marker vesicular acetylcholine transporter in the region. Rapid pacing revealed RVOT susceptibility to both concordant and discordant alternans. Investigation into transmural arrhythmia dynamics showed that arrhythmia wavefronts and phase singularities (rotors) were relatively more organized in the endocardium than in the epicardium (p=0.006). Moreover, there was a weak but positive spatio-temporal autocorrelation between epicardial and endocardial arrhythmic wavefronts and rotors. Transcriptome analysis (n=10 hearts) suggests a trend that MAPK signaling, calcium signaling, and cGMP-PKG signaling are among the pathways that may be enriched in the male RVOT, whereas pathways of neurodegeneration may be enriched in the female RVOT.

Conclusions: Human RVOT electrophysiology is characterized by shorter action potential duration relative to the RVAR. Cholinergic RV stimulation attenuates the arrhythmogenic effects of adrenergic stimulation, including increase in frequency of PVCs and shortening of wavelength. RV arrhythmia is characterized by positive spatial-temporal autocorrelation between epicardial-endocardial arrhythmic wavefronts and rotors that are relatively more organized in the endocardium.

Graphical Abstract

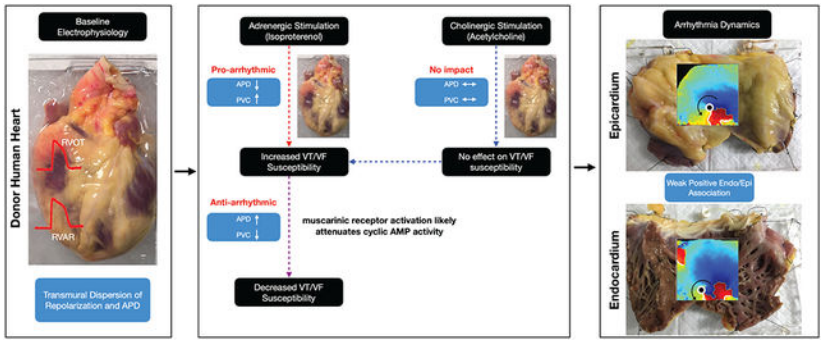

Keywords

Right ventricle; Right ventricular outflow tract; Right ventricular apical region; Premature ventricular contraction; Arrhythmia; Acetylcholine; Isoproterenol; Autonomic modulation; RNA-Seq; Immunohistochemistry; Optical mapping; Electrical mapping; Donor human hearts

Subject terms

Right ventricle (RV); Right ventricular outflow tract (RVOT); Right ventricular apical region (RVAR); Sympathetic; Parasympathetic; Arrhythmia; Alternans; Premature ventricular contractions (PVCs); Electrogram; Transcriptomics; Electrophysiology; Vesicular acetylcholine transporter (VAChT); Monomorphic ventricular tachycardia (MMVT); Ventricular Fibrillation (VF); Donor human hearts

Introduction

The right ventricular outflow tract (RVOT) is a dominant site of origin of PVCs and ventricular tachyarrhythmias including Brugada syndrome, idiopathic ventricular arrhythmias (IVA), and arrhythmogenic right ventricular cardiomyopathy among others[1,2]. Anatomically, the RVOT is a thin, smooth-walled, tubular structure located between the pulmonary artery and inlet and apical components of the right ventricle. The tissue structure is interspersed with heterogenous distribution of fibrous and fat tissue[3,4] and comprises a complex three-dimensional network of cardiac fibers arranged circumferentially in the sub-epicardium and longitudinally in the sub-endocardium[5]. Moreover, the RVOT-pulmonary root junction is characterized by multiple tissue types including myocardium, valve and smooth muscle tissue, with the myocardium of the free-standing subpulmonary infundibulum commonly supporting the bases of the three pulmonary sinuses[6]. Given the complex anatomical makeup and the presence of endocardial Purkinje network[7], the RVOT could be predisposed to arrhythmogenesis, as suggested by the observation that nearly 80% of IVAs originate in the RVOT[8]. While there have been basic RVOT studies in mice[9,10], rabbit[11,12], porcine[13], and canine[14,15] animal models, the electrophysiological and arrhythmogenic profile of healthy human RVOT remains poorly studied.

The autonomic nervous system (ANS) plays an important regulatory role in cardiac physiology, and the dysfunction of the ANS associated with sympathovagal imbalances has been linked to cardiac arrhythmias[16,17]. While sympathetic modulation affects both the atria and the ventricles, the current paradigm suggests that the parasympathetic control is limited to the atria and that direct parasympathetic modulation of the ventricles is insignificant[18]. Evidence suggests the presence of cholinergic innervation in the ventricles in various species,[19,20] but the functional significance of direct parasympathetic influence on ventricles is not well-established or characterized.

Both focal and reentrant mechanisms both play a role in arrhythmogenesis, with reentry believed to be the primary mechanism of maintenance of sustained ventricular arrhythmias,[21] and focal sources serving as triggers. However, controversy remains on the mechanism of reentrant arrhythmia: is it driven by multiple wavelets or a single mother rotor[22]? Recent studies have also suggested that endocardial and epicardial dissociation may play a role in the maintenance of atrial arrhythmias[23]. However, the role endocardial-epicardial dissociation in the maintenance of ventricular arrhythmias is not well-characterized.

In this study, we aimed to fill the existing knowledge gap in characterization of human RVOT electrophysiology using dual-sided (epicardial and endocardial) optical and electrical mapping of the right ventricle (RV) from donor human hearts, and to characterize transcriptome and proteins expression in combination with RNAseq and immunohistochemistry, respectively. Using these techniques, we provide novel functional, structural, and transcriptomic profile of non-pathological human RVOT.

Materials and Methods

The data, methods, and study materials will be made available for other researchers upon request for the purposes of developing new methods of analysis, reproducing the results or replicating the procedure. Detailed description of the materials and methods are available in the supplementary materials.

Study design

All studies (n=30) using de-identified human heart tissue were approved by the Institutional Review Board at the George Washington University and University of California Los Angeles. In total for this study, we procured 29 de-identified donor human hearts from Washington Regional Transplant Community. One additional donor heart was procured through the UCLA Cardiac Arrhythmia Center in Los Angeles, California. All hearts were arrested using ice-cold cardioplegic solution in the operating room and transported to the laboratory for dissection and subsequent electrophysiology, transcriptome, and immunostaining studies. A complete list of hearts with available clinical information is shown in Supplementary Figure I.

This was a prospective, non-randomized study, and the investigators were not blinded to the data. Three donor hearts (Group 0) were used to conduct exploratory research including development of study protocol and the techniques for RVOT wedge dissection, cannulation, and perfusion. Donor hearts were grouped to investigate the effects of cholinergic and adrenergic modulation using optical mapping. Group 1 (n=7; male=3, female=4) donor hearts were used to study the effects of cholinergic and adrenergic stimulation in isolation. Group 2 (n=6; male=3, female=3) was used to evaluate the effects of cholinergic stimulation in donor hearts already subjected to adrenergic stimulation. Since fresh tissue samples could not be extracted from Groups 1 and 2, additional Group 3 donor hearts were used to collect tissue for RNA sequencing (n=10; male=5, female=5) and immunostaining (n=4; male=1, female=3) studies. Group 3 was not subjected to functional studies in order to avoid likely changes in transcriptome caused by in vitro perfusion. While optical mapping was the primary modality for functional studies, we also conducted simultaneous optical and electrical mapping in 3 donor hearts to validate optical mapping with a clinically relevant electrical mapping.

All data and software used for functional, transcriptomic, and immunostaining studies will be made available through the online repository at the George Washington University.

Experimental preparation and study protocol

Dual-sided (epicardial and endocardial) optical and electrical mapping experiments were conducted in RVOT preparations from donor human hearts (Figure 1A). To prepare the RVOT wedge preparation, the aorta and the pulmonary artery were dissected open to expose and isolate the right and left coronary arteries for cannulation. Most of the atria, the left ventricle (LV), and the posterior RV were removed to expose the anterior RV and the RVOT surface area. The remaining vessel branches were tied off. The RVOT preparation was stretched across a frame and secured to pull it flat (Figure 1B). The tissue was

suspended vertically in a bath to allow optical access to both the endocardial and epicardial surface and immobilized by blebbistatin (10-15 μM) to suppress motion artifacts in optical recordings, without adverse electrophysiological effects[24]. Di-4-ANBDQBS was used to map transmembrane potential as previously described[25].

Tissue was paced from the endocardium using a dynamic restitution protocol (S1S1) to assess rate dependence of action potential duration (APD). Briefly, the S1S1 protocol entails pacing the tissue for at least 60 beats at constant cycle length (S1S1), and then repeating the process by progressively shortening the S1-S1 intervals. This restitution protocol was executed after each treatment. For Group 1, the tissue was treated with acetylcholine (100 μM) and the restitution protocol repeated. Following that, acetylcholine was washed out, and the tissue was treated with isoproterenol (100 nM). The restitution protocol was repeated until arrhythmia was induced (Figure 1C). For Group 2, the tissue was first treated with isoproterenol (100 nM) and the restitution protocol repeated. The tissue was then subjected to acetylcholine (100 μM) treatment, while still under the influence of sympathetic stimulation (no washout of isoproterenol). In case the S1S1 restitution protocol alone was unable to induce arrhythmia, burst pacing (50Hz) in combination with pinacidil (50 μM) was used for arrhythmia induction. Only in two cases (D3 and D10) we were unable to induce arrhythmia. All arrhythmia inductions were sustained and lasted for at least 15 minutes. We chose an aggressive arrhythmia induction protocol as VT is only occasionally initiated by premature ventricular contractions (PVCs) originating from the RVOT[26].

Optical Cardiac Mapping

Optical action potentials were mapped from approximately 7cm x 7cm field of view from the two surfaces (epicardium and endocardium) using two MiCAM05 (SciMedia, CA) CMOS cameras (100 x 100 pixels). All optical signals were processed in MATLAB-based custom open-source software RHYTHM. Activation times were determined by calculating the time of dF/dt_{max}, which corresponds to the steepest segment of the optical action potential upstroke (Supplementary Figure IIA). APD was calculated at 80% repolarization (APD80). To measure the extent of spatial organization during ventricular tachyarrhythmia, indices including dominant frequency (DF), regularity index (RI), and organization index (OI) were evaluated for each pixel[27]. To evaluate the complexity of arrhythmias including wavefront dynamics, phase singularity dynamics and endocardial-epicardial dissociation dynamics, the optical signals were transformed into the phase domain using the Hilbert Transform (Supplementary Figure IIB).

Wavefronts (WF) were defined as the isophase lines along $\varphi=\pi/2$[28]. The number of discrete wavefronts were calculated for each field of view and tracked over its lifespan. Wavefronts smaller than 20 pixels (approximately 14mm) were treated as noise and not included in the analysis. Wavefront collision was defined as a phenomenon wherein two wavefronts collided with each other and merged into a single wavefront (Video I). Wavefront fractionation was defined as a phenomenon where a single wavefront would split into two wavefronts (Video II). A collision or a fractionation (wavefront splitting) marked the end of the lifespan of a wavefront. Alternately, wavefront tracking was also terminated if the wavefront moved past the field of view, fell below the 20-pixel threshold or expired (Video III). Wavefronts

were also tracked for multiplicity and repeatability[29]. Multiplicity was defined as an index of number of unique wavefront pathways in an overall activation pattern. Repeatability was defined as measure of the number of times a wavefront propagation over a pathway was repeated (Video IV). Phase singularities (PS) were calculated as nonzero topological charges constrained to the isophase wavefronts within 3-pixel radius (approximately 2mm) in each frame. PS meandering (total distance traveled) and PS displacement (shortest path between initial and final position) were calculated by tracking individual PS trajectories across their lifespans. To explore the endocardial-epicardial arrhythmia dissociation dynamics, wavefronts, and PS between the two surfaces were compared using spatio-temporal autocorrelation analysis. Epicardial and endocardial DF, RI, and OI were also compared at each pixel location to compute the Jaccard similarity index[30].

Electrical Cardiac Mapping

To establish clinical relevance of optical mapping we applied simultaneous electrical and optical cardiac mapping in donor hearts (n=3; male=2, female=1). Briefly, two stretchable passive electrode arrays were used for epicardial and endocardial electrical mapping. Each array (3cm x 4cm) had 64 electrodes arranged in an 8x8 matrix with interelectrode distance of approximately 3-4mm and electrode diameter of approximately ~1mm. Fabrication of the electrode array was done at Northwestern University as described ealier[31]. A custom-printed circuit board (PCB) was fabricated at Duke University[32] for connecting the electrode array to a data acquisition system (1024-channel RHD recording system, Intan Technologies, CA). The electrical and optical data acquisition systems were compared to enable synchronized measurements of electrical and optical signals. All the unipolar electrical signals were processed in MATLAB version 2020a. The local activation times were determined by calculating the time of dV/dt_{min}. which corresponds to the steepest downward slope in the activation complex. The local repolarization times were determined by calculating T_{up}, the point in the T wave with the maximum upward slope (Supplementary Figure IIC). Activation-recovery interval (ARI), a surrogate marker of APD, was then computed as the interval between local activation and repolarization time[33] and is assumed to occur near APD50[34].

Transcriptome

Tissues from human RVOT and RV apical region, separated into epicardium and endocardium (total hearts=10; male=5, female=5; 4 tissue samples from each heart) were collected for subsequent RNA extraction. RNA sequencing was performed with Illumina HiSeq using paired-end 150 reads (Novogene). DESeq2 was used for differential gene expression (10.1186/s13059-014-0550-8). Differentially expressed genes (DEGs) cutoff was at $padj<0.05$. Enrichment analysis on DEGs was performed with goana (10.12688/f1000research.8987.2) for gene ontology and clusterProfiler (10.1089/omi.2011.0118) for KEGG.

Immunostaining

Briefly, fixed specimens of the human heart RVOT were shipped to Eastern Tennessee State University (ETSU) at 4 °C in PBS containing 20% sucrose and 0.02% sodium azide. Slide-mounted tissue sections were immunostained at room temperature for specific neural

markers using standard methods of ABC immunohistochemistry. Primary antibodies used included rabbit anti-vesicular acetylcholine transporter (VAChT, Synaptic Systems, Cat. No. 139103, 1:500), sheep anti-tyrosine hydroxylase (TH, Millipore Cat. No. AB1542, 1:500), or rabbit anti-protein gene product 9.5 (PGP9.5, Abcam Cat. No. ab108986, 1:2000). Nerve density was calculated as the area occupied by nerves as a percentage of the entire image area and reported as % area. Data was analyzed and graphed using Prism version 8.4.3 (GraphPad Software, CA).

Statistical analysis

All means characterizing the spatial average of a single study are represented as sample mean±SD. All means that characterize average trends across the cohort of donor hearts are reported as sample mean±SEM. Repeated measures ANOVA (one-way or two-way) with multiple comparisons and post hoc Holm-Sidak or Tukey's Honest Significant Difference (THSD) multiple comparison test was used for APD and PVC comparisons, respectively. Two-tailed paired t test was used for comparison between epicardial and endocardial WF and PS metrics. Significance was defined as $p<0.05$.

Results

Cardiac mapping of human RVOT reveals transmural APD and repolarization gradient

To determine whether the RVOT had distinctive electrophysiological features relative to the RVAR, we conducted cardiac mapping studies using RV tissue from 16 donor human hearts. The epicardial and endocardial activation, repolarization (REP80), and action potential duration maps, as well as sample optical action potentials (OAP) from a representative donor heart (D11) paced at 60BPM (Figure 2A) depicts the underlying repolarization dispersion and APD dispersion. For three donor hearts, we also conducted simultaneous electrical and optical mapping studies to evaluate the feasibility of dual modality mapping. The representative (D14) activation maps from simultaneous electrical and optical mapping paced at 120 BPM showed similar profile (Figure 2B). Moreover, the ARI calculated from time aligned electrograms (EGM) correlated with APD50 (epicardium $r= 0.81$, endocardium $r = 0.92$, Pearson correlation). There was no statistically significant difference between the ARI and the APD50 restitution curves (Supplementary Figure III). These data suggest that simultaneous electrical and optical mapping can be employed as a viable technique to generate a richer set of strongly correlated data. The APD80 restitution curves provide a statistical summary for each region (RVOT or RVAR) as well as the overall RV in the epicardium and the endocardium (Figure 2C). We noted shorter action potentials in the RVOT relative to the RV apical region ($p_{epi} < 0.0001$ and $p_{endo} < 0.0001$, repeated measures 2-way ANOVA). We also found shorter APs in the RVOT epicardium relative to the RVOT endocardium ($p = 0.0016$, repeated measures 2-way ANOVA). Moreover, there was a general trend with female APD80 being longer than male APD80, especially at lower heart rates, however, it was not statistically significant. Similarly, while the female REP80 dispersion and APD80 dispersion trended to be longer than the male counterparts, they were not statistically significant. These results suggest that RVOT drives the transmural dispersion of repolarization and the transmural APD dispersion under normal physiological conditions.

Cholinergic stimulation attenuates effects of adrenergic stimulation

To determine the role of parasympathetic stimulation in ventricular electrophysiology, we compared the electrophysiological response of RV subjected to acetylcholine (100 μM) treatment in absence of sympathetic stimulation (Group 1) with the electrophysiological response of RV pre-treated with isoproterenol (100 nM) and subsequently subjected to acetylcholine (100 μM) stimulation (Group 2). In Group 1 donor hearts, treatment with acetylcholine had no effect on APD relative to baseline conditions. Moreover, after acetylcholine was washed out, treatment with isoproterenol shortened APD as expected (Figure 3A, Supplementary Figure IVA). In comparison, Group 2 donor hearts, were treated with isoproterenol first, which resulted in shortening of APD. However, while still under the influence of isoproterenol, additional treatment with acetylcholine resulted in prolongation of the APD (p_{epi} = 0.015, p_{endo} = 0.029, repeated measures 2-way ANOVA) back towards baseline conditions (Figure 3B, Supplementary Figure IVB). APD80 maps (paced at 60BPM) and the corresponding sample OAPs from a representative Group 2 donor heart (D11) highlights the initial shortening of APs in response to isoproterenol (100 nM) stimulation and subsequent lengthening of APs reverting to near baseline conditions, upon treatment with acetylcholine (100 μM) (Figure 3C). We also counted nerve density distribution in RVOT tissue samples from four additional donor hearts using immunohistochemical staining, which showed the presence of VAChT-positive, PGP9.5-positive, and TH-positive nerve densities in both the sub-epicardial and the sub-endocardial regions (Figure 3D, Supplementary Figure V).

Given that adrenergic stimulation promotes PVCs it is possible that additional cholinergic stimulation could have inverse effects on PVCs as seen previously with APD. To investigate further this idea, we tracked the frequency of PVCs in donor hearts from both groups (Figure 4A). In Group 1, acetylcholine (100 μM) by itself had no effect on the frequency of PVCs compared to baseline. In contrast, treatment with isoproterenol (100 nM), after washout of acetylcholine noticeably increased the frequency of PVCs (p = 0.036, ordinary ANOVA). In Group 2 hearts, initial treatment with isoproterenol (100 nM) increased the frequency of PVCs (p = 0.003, ordinary ANOVA), as expected. However, additional treatment with acetylcholine (100 μM) reduced the frequency of PVCs (p = 0.034, ordinary ANOVA). The effects were consistent across both male and female donor hearts from both groups. However, we did not find any statistically significant sex-related differences in frequency of PVCs in response to either sympathetic and/or parasympathetic stimulation, presumably due to age of the hearts studied. Taken together, these results show that while parasympathetic stimulation by itself has no statistically significant effect on ventricular electrophysiology, in the presence of adrenergic stimulation, cholinergic stimulation attenuates the effects on APD and PVC frequency.

To investigate the nature of arrhythmia susceptibility, RV tissue from 13 donor hearts were treated with isoproterenol (100 nM) and then subjected to S1S1 restitution stimulation to induce arrhythmias, which also triggered concordant or discordant alternans, dependent on frequency of stimulation. An example of discordant APD50 alternans (Figure 4B) induced at 240BPM from a representative donor heart (D10) as well as an example of concordant alternans (Supplementary Figure VIA) induced at 300BPM from another representative

donor heart (D11) highlights the heterogeneous spatial distribution of alternans. In general, alternans appeared slightly more prevalent in the endocardium in comparison with the epicardium. Incidences of concordant alternans were relatively more frequent than discordant alternans (Supplementary Figure VIB). Moreover, discordant alternans occurred at higher frequencies in comparison with concordant alternans. Finally, the RVOT region appeared to be slightly more susceptible to the alternans in comparison with the rest of the RV. Our data suggests that RVOT is susceptible to both concordant and discordant alternans, which may be linked to the intrinsic transmural dispersion of repolarization as well as transmural APD dispersion and result in vulnerability to arrhythmias.

Arrhythmia wavefront and phase singularity dynamics

To get further insight into the transmural dynamics of RV arrhythmias, RV tissue was subjected to pharmacological arrhythmia promotion in combination with S1S1 protocol and, failing that, a 50 Hz burst pacing protocol. We induced sustained arrhythmias (lasting longer than 15 mins) in 12 donor hearts with three of them categorized as monomorphic ventricular tachycardia (MMVT). Representative arrhythmia phase data from donor heart (D14) showed reentrant MMVT and was characterized by a scroll wave, anchored by two phase singularities, one each on the epicardium and the endocardium respectively (Figure 5A, Video V). The DF (epicardium 6.98 ± 1.13 Hz, endocardium 7.12 ± 0.67 Hz), RI (epicardium 0.75 ± 0.18, endocardium 0.78 ± 0.14), and OI (epicardium 0.83 ± 0.16, endocardium 0.90 ± 0.14) maps reflected organized nature of MMVT (Figure 5B). Arrhythmic wavefronts were characterized by collisions (epicardium 28.77%, endocardium 23.77%) and fractionations (epicardium 27.10%, endocardium 25.85%) but also showed high degree of repeatability (epicardium 67.95%, endocardium 82.72%) (Figure 5C). The average wavefront size was larger, but the average wavefront duration was smaller in the epicardium (size 4.29 ± 4.11 cm, duration 4.3 ± 7.7 ms) in comparison with the endocardium (size 3.64 ± 3.09 cm, duration 6.5 ± 10.2 ms). Moreover, the number of wavefronts was also larger in the epicardium (epicardium 8.55 /cm^2s, endocardium 5.06 /cm^2s). Analysis of epicardial and endocardial phase singularities (PS) showed that the average duration of PS was larger in the endocardium (epicardium 37.3 ± 27.3 ms, endocardium 43.8 ± 28.8 ms) (Figure 5D). Moreover, only a small fraction of PS was considered stable, defined as lasting at least one cycle length in duration (epicardium 2.25%, endocardium 2.01%). PS meandering (epicardium 1.36 ± 0.72 cm, endocardium 1.31 ± 0.68 cm) was slightly longer in the epicardium. Spatio-temporal autocorrelation analysis showed weak positive association between epicardial and endocardial wavefronts (28.4% of wavefronts followed similar trajectories) and PS (38.5% similar trajectories) (Figure 5E). Dynamic time warp (DTW) was used to quantify the similarity between epicardial and endocardial wavefront temporal sequences and showed relatively higher incongruence (DTW distance = 46) compared to during pacing (DTW distance = 5) (Supplementary Figure VII). Moreover, the local epicardial and endocardial DF was highly congruent (96.6% similar). These results suggest that MMVT in donor human RV/RVOT is driven by a relatively small number of highly repeatable wavefronts and phase singularities that are reentrant in nature and have high degree of regularity.

Representative arrhythmia phase data from donor heart (D4) shows ventricular fibrillation also with an instance of scroll wave (Figure 6A, Video VI). The DF (epicardium 6.96 ± 4.81 Hz, endocardium 8.54 ± 3.61 Hz), RI (epicardium 0.32 ± 0.17, endocardium 0.38 ± 0.15), and OI (epicardium 0.45 ± 0.17, endocardium 0.48 ± 0.22) maps reflected the relatively less organized VF wavefronts in comparison with that seen in MMVT (Figure 6B). Analysis of epicardial and endocardial wavefronts showed high degree of multiplicity (epicardium 71.11%, endocardium 70.99%) and lower degree of repeatability (epicardium 28.89%, endocardium 29.01%) in comparison with MMVT (Figure 6C). The average size was larger, but the average duration was smaller in the epicardial wavefronts (size 3.44 ± 2.95 cm, duration 3.71 ± 5.98 ms) in comparison with the endocardial wavefronts (size 3.10 ± 2.28 cm, duration 4.80 ± 7.35 ms). Moreover, the number of wavefronts was also larger in the epicardium (epicardium 19.59 /cm^2s, endocardium 15.84 /cm^2s) and both were larger than compared with MMVT wavefronts. Analysis of epicardial and endocardial PS showed that the average duration of PS was also larger in the endocardium (epicardium 33.4 ± 17.98 ms, endocardium 38.97 ± 24.57 ms) (Figure 6D). In addition, relatively smaller fraction of PS was stable (epicardium 0.61%, endocardium 1.48%) in comparison with MMVT. PS meandering (epicardium 1.28 ± 0.64 cm, endocardium 1.15 ± 0.66 cm) and displacement (epicardium 0.35 ± 0.21 cm, endocardium 0.33 ± 0.19 cm) were also longer in the epicardium. Spatio-temporal autocorrelation analysis showed weaker positive association between epicardial and endocardial wavefronts (16.5% of wavefronts followed similar trajectories) and PS (33.17% similar trajectories) in comparison with MMVT (Figure 6E). These results suggest that VF in donor human RV/RVOT is driven by a relatively larger number of irregular and less organized wavefronts and PS that still appear to be reentrant in nature.

The statistical summary of arrhythmia dynamics from twelve donor hearts suggest that the endocardial arrhythmic wavefronts are relatively more regular ($p = 0.0026$, paired t test) and organized ($p = 0.0058$, paired t test) than seen in the epicardium (Figure 7B-C). However, we do not observe any statistically significant sex specific differences relative to arrhythmia wavefront organization (Supplementary Figure VIIIB-C). Epicardial wavefront size is larger ($p = 0.0034$, paired t test) and so is wavefront count ($p = 0.0003$, paired t test) in comparison with endocardial wavefronts (Figure 7D-E), whereas the endocardium is characterized by longer wavefront duration ($p=0.0001$, paired t test) (Figure 7F). Moreover, epicardial wavefronts are characterized more fractionations in comparison with the endocardium (Figure 7G). PS duration ($p < 0.0001$, paired t test) are longer in the endocardium than seen in the epicardium (Figure 7L), whereas the epicardium is characterized by larger PS meandering and displacement (Figure 7M-N). Taken together, these results provide further statistical evidence that the arrhythmia in the endocardium is relatively more organized than in the epicardium.

Sex-specific differences in the human RVOT transcriptome

We sought to get insight into the regulatory features of the RVOT by determining the transcriptome profile of RVOT and RV apical region tissue from 10 donor human hearts using bulk RNA-seq. Principal component analyses showed that the tissue samples were clustered together by sex along the first principal component, which accounted

for 26% of the observed variance (Figure 8A). Bioinformatic analysis showed that sex altered expression of 261 genes in the RVOT (Figure 8B). To further elucidate sex and location (RVAR vs RVOT, epicardium vs endocardium) specific differences, we performed hierarchical clustering of both genes and the samples based on the gene expression profile (DEGs) in the gene expression matrix, identifying the top 20 genes (Figure 8C). Further GO analysis showed that these sex-regulated genes are mainly involved in immunoglobin complex and humoral immune response etc., in case of females and demethylase activity and demethylation etc., in case of males (Figure 8D). KEGG analysis revealed the top 16 KEGG-annotated pathways enriched for DEGs expressed in male and female RVOT (Figure 8E). Among them, MAPK signaling[35], calcium signaling[36], and cGMP-PKG signaling[37] pathways, which were enriched in male RVOT, have been reported to be involved in cardiac hypertrophy and cardiac electrophysiological remodeling. Incidentally, neurodegeneration pathways were enriched in female RVOT. These differences were not as pronounced when comparing sex specific differences in the RV apical region (Supplementary Figure IX). Our results suggest a trend that MAPK signaling, calcium signaling, and cGMP-PKG signaling pathways could be linked with the sex-specific electrophysiological differences seen in the RVOT.

Discussion

In this study, we studied donor human hearts to assess the basic electrophysiology and transcriptome of human RVAR and RVOT tissue and investigate the effects of autonomic modulation on arrhythmia susceptibility, while also leveraging this data to characterize transmural arrhythmia dynamics. We showed that RVOT is characterized by shorter action potentials in comparison with the RVAR, which is evident in both transmural dispersion of repolarization and APD. We also showed that cholinergic stimulation in isolation has no effect on the RV electrophysiology. However, in the presence of adrenergic stimulation, additional cholinergic stimulation counteracts the sympathetic effects by attenuating both APD shortening and the frequency of PVCs. Finally, we also showed that RV arrhythmia dynamics is characterized by reentry, which is relatively more organized in the endocardium in comparison with the epicardium.

Our data support the existence of spatial heterogeneity in repolarization and APD between epicardial and endocardial RVOT and the RVAR under physiological conditions. The reasons for this heterogeneity remain unclear but could be associated with one or more of conduction velocity heterogeneities or spatial heterogeneities of calcium dynamics and the ionic currents in the sarcolemma that drive repolarization phase of action potentials, or intercellular uncoupling. Work done by Boukens et al in mice suggests that the slow conducting phenotype of the embryonic RVOT is maintained in adult heart resulting in lower conduction reserve in the RVOT relative to RV[10]. Our transcriptomic analysis of RVAR and RVOT tissue did not reveal any statistically significant differences in the calcium, potassium or gap junction channel expressions. However, work by Gaborit et al on non-diseased human hearts suggests that basal epicardium is characterized by higher expression of genes related to calcium handling (Cav1.2 and SERCA2), whereas the basal endocardium has higher expression of sodium channels (Nav1.5, Navβ1)[38]. There is also literature evidence to suggest that in healthy human hearts, RV contains relatively larger collagen content and fat

relative to the LV[3]. Moreover, if non-vascular intramural clefts seen in the mouse RVOT[9] are present in the human RVOT, it could also facilitate subtle intercellular uncoupling. While the precise mechanisms remain unelucidated, our results encourage future studies to understand the specific role of each mechanism.

Our study showed that acetylcholine by itself had no effect on APD or the frequency of PVCs in the RV, unlike isoproterenol, which shortened APD and increased the frequency of PVCs. However, acetylcholine in presence of adrenergic stimulation mediated reversal of isoproterenol shortened APD and decreased the frequency of PVCs induced by isoproterenol. Moreover, immunohistochemistry also confirmed ventricular cholinergic innervation, revealing the presence of VAChT nerve densities across the RVOT transmural wall. Vagal nerve stimulation (VNS) has been reported in preclinical and clinical studies to have anti-arrhythmic effects, especially in the setting of acute and chronic myocardial ischemia and infarction, which is often associated with imbalance in autonomic modulation in favor of sympathetic hyperactivity[39-43]. The presence of vagal innervation in the ventricle has been confirmed by others and it has also been suggested that muscarinic receptors on adrenergic nerve terminals could attenuate norepinephrine release, resulting in parasympathetically mediated inhibitory effects on cardiac sympathetic activity[44-46].

Our data also revealed that RV/RVOT is characterized by complex transmural arrhythmia dynamics that can extend from a relatively few organized and stable reentrant rotors as seen during MMVT to many disorganized and transient rotors, that also exhibited reentry as seen during VF. Compared to the endocardium, the epicardium had more wavefronts per unit area and per unit time and more wavefront fractionations, which could be associated with the fat accumulation on the epicardial surface. However, the endocardium was characterized by longer wavefront duration and PS duration, larger regularity and organizational index, and shorter PS meandering and PS displacement. Taken together, these metrics suggest that the endocardium has relatively more organized and stable arrhythmia dynamics relative to the epicardium. The relative disorganization of arrhythmias on the epicardium could be associated with the accumulation of epicardial adipose tissue (EAT), which has been associated with electrical and structural remodeling in the atria[47]. In addition, there was a weak positive spatio-temporal association between epicardial and endocardial wavefronts and PS and could be characterized as three-dimensional scroll waves with colocalized rotors extending out onto both surfaces. Our findings suggest reentry as the primary mechanism driving the arrhythmia dynamics in RV. In case of low complexity arrhythmias such as MMVT, the reentrant arrhythmia appears to be characterized by a small number of stable rotors. Furthermore, in case of high complexity arrhythmias such as VF, the reentrant arrhythmia appears to be driven by multiple propagating wavelets. Taken together, we believe the arrhythmia dynamics lie on a spectrum with stable reentrant rotors[21] governing low complexity arrhythmias on end, and multiple wavelets[48] driving high complexity fibrillation dynamics on the other end. Incidentally, the average displacement of the rotor (epi 0.32 ± 0.01 cm, endo 0.31 ± 0.02 cm) also suggests the minimal spatial resolution needed to accurately localize arrhythmia drivers.

Ventricular tachycardias originating in the RVOT are commonly associated with focal mechanisms, including enhanced automaticity and cAMP-mediated triggered activity[2].

Moreover, the ectopic activity in the RVOT can be facilitated by catecholamines, but seldom results in sustained VT, especially in non-pathological hearts. In our study, we combined infusion with isoproterenol with concurrent rapid pacing to achieve sustained VT. It is likely that in failing hearts, the ectopic activity is more likely to lead to sustained VT and will be investigated in the future.

Limitations

Our work presents several limitations. First, the cohort of donor hearts procured for this study had unavoidable high variability given the different co-morbidities present (e.g., hypertension, diabetes, asymptomatic onset of cardiovascular disease, perhaps due to age etc.,). Most of the hearts we received were rejected for transplantation due to age restriction and we had limited information available on the exact health status. As such we cannot discount the effect of co-morbidities that may be present. Even so, the donor hearts represent as close to normal human physiology as is possible in a basic research setting. Second, the fat accumulation on the epicardium as well as the presence of endocavitary structures (e.g., papillary muscles, moderator band, and trabeculations) made it difficult to measure conduction velocity with precision. Therefore, the role of conduction velocity heterogeneity was not explored. Third, we did not quantify the fibrous and fatty infiltration or the number of non-vascular clefts in the RVOT tissue, which could potentially play a role in the spatial heterogeneities of APD and repolarization. Fourth, we did not investigate the role of Purkinje fibers in the arrhythmia dynamics, which could contribute to arrhythmia through a combination of triggered activity and reentrant wavefronts[49]. Fifth, recent studies[50,51] have suggested that idiopathic VF seen in structurally normal hearts may result from structural abnormalities including diffuse fibrosis and increased collagen content in the myocardium that may not be readily detected by standard clinical imaging modalities. While the donor hearts used in this study may have developed age related fibrosis, we did not explore the role of subtle structural abnormalities in arrhythmogenesis.

Conclusions

In this report we show that human RVOT electrophysiology is characterized by shorter action potentials relative to the RVAR resulting in spatial heterogeneity of repolarization and APD and potentially creating a substrate for arrhythmia vulnerability. We also report that cholinergic stimulation attenuates the arrhythmogenic effect of adrenergic stimulation by reversing APD shortening and decreasing the frequency of PVCs. Finally, we also show that RV arrhythmia is characterized by reentry associated with a small but stable group of rotors as seen in MMVT or multiple transient wavelets as seen in VF. Furthermore, the epi/endo arrhythmia dynamics is characterized by weak positive spatial-temporal autocorrelation between epicardial and endocardial wavefronts and rotors that are relatively more organized and stable in the endocardium.

Supplementary Material

Refer to Web version on PubMed Central for supplementary material.

Acknowledgments:

The authors thank Allan Li, Brianna Cathey, Sharon George, Rose Yin, Zach Li, Micah Madrid, Istvan Koncz for their excellent technical assistance.

Sources of Funding:

This work was supported from NIH to IE and KA (R44 HL139248, 3OT2OD023848 and 1K99HL148523-01A1), NIH to PH (F32HL152609), American Heart Association 2019 CENTER Arrhythmias SCD Strategically Focused Research Network to IE and Leducq Foundation grant RHYTHM to IE.

Non-standard Abbreviations and Acronyms

ANS	Autonomic nervous system
APD80	Action potential duration at 80% repolarization
ARI	Activation recovery interval
cAMP	Cyclic adenosine 3’,5’-monophosphate
cGMP-PKG	Cyclic guanosine 3’,5’-monophosphate dependent protein kinase G
DEG	Differentially expressed genes
DF	Dominant frequency
DTW	Dynamic time warp
EGM	Electrograms
GO	Gene ontology
IVA	Idiopathic ventricular arrhythmia
KEGG	Kyoto encyclopedia of genes and genomes
LV	Left ventricle
MAPK	Mitogen-activated protein kinase
MMVT	Monomorphic ventricular tachycardia
OAP	Optical action potential
OI	Organization index
PGP9.5	Protein gene product 9.5
PS	Phase singularity or rotor
PVC	Premature ventricular contractions
REP80	Action potential repolarization at 80%
RI	Regularity index

RV	Right ventricle
RVAR	Right ventricular apical region
RVOT	Right ventricular outflow tract
S1S1	Basic pulse pacing protocol
Th	Tyrosine hydroxylase
VAChT	Vesicular acetylcholine transporter
VF	Ventricular fibrillation
VT	Ventricular tachycardia
WF	Arrhythmic wavefronts

References:

1. Blok M, Boukens BJ. Mechanisms of arrhythmias in the brugada syndrome. Int J Mol Sci. 2020;21:1–20.
2. Lerman BB, Cheung JW, Ip JE, Liu CF, Thomas G, Markowitz SM. Mechanistic subtypes of focal right ventricular tachycardia. J Cardiovasc Electrophysiol. 2018;29:1181–1188. [PubMed: 29659078]
3. Miles C, Westaby J, Ster IC, Asimaki A, Boardman P, Joshi A, Papadakis M, Sharma S, Behr ER, Sheppard MN. Morphometric characterization of collagen and fat in normal ventricular myocardium. Cardiovasc Pathol. 2020;48:107224. [PubMed: 32480283]
4. Basso C, Thiene G. Adipositas cordis, fatty infiltration of the right ventricle, and arrhythmogenic right ventricular cardiomyopathy. Just a matter of fat? Cardiovasc Pathol. 2005;14:37–41. [PubMed: 15710290]
5. Ghonim S, Voges I, Gatehouse PD, Keegan J, Gatzoulis MA, Kilner PJ, Babu-Narayan SV. Myocardial Architecture, Mechanics, and Fibrosis in Congenital Heart Disease. Front Cardiovasc Med. 2017;4:30. [PubMed: 28589126]
6. Asirvatham SJ. Correlative anatomy for the invasive electrophysiologist: Outflow tract and supravalvar arrhythmia. J Cardiovasc Electrophysiol. 2009;20:955–968. [PubMed: 19490263]
7. De Almeida MC, Stephenson RS, Anderson RH, Benvenuti LA, Loukas M, Aiello VD. Human subpulmonary infundibulum has an endocardial network of specialized conducting cardiomyocytes. Heart Rhythm. 2020;17:123–130. [PubMed: 31377422]
8. Kamakura S, Shimizu W, Matsuo K, Taguchi A, Suyama K, Kurita T, Aihara N, Ohe T, Shimomura K. Localization of optimal ablation site of idiopathic ventricular tachycardia from right and left ventricular outflow tract by body surface ECG. Circulation. 1998;98:1525–1533. [PubMed: 9769306]
9. Kelly A, Salerno S, Connolly A, Bishop M, Charpentier F, Stølen T, Smith GL. Normal interventricular differences in tissue architecture underlie right ventricular susceptibility to conduction abnormalities in a mouse model of Brugada syndrome. Cardiovasc Res. 2018;114:724–736. [PubMed: 29267949]
10. Boukens BJ, Sylva M, de Gier-de Vries C, Remme CA, Bezzina CR, Christoffels VM, Coronel R. Reduced sodium channel function unmasks residual embryonic slow conduction in the adult right ventricular outflow tract. Circ Res. 2013;113:137–141. [PubMed: 23661717]
11. Ou B, Nakagawa M, Kajimoto M, Nobe S, Ooie T, Ichinose M, Yonemochi H, Ono N, Shimada T, Saikawa T. Heterogeneous expression of connexin 43 in the myocardium of rabbit right ventricular outflow tract. Life Sci. 2005;77:52–9. [PubMed: 15848218]
12. Zaitsev AV, Torres NS, Cawley KM, Sabry AD, Warren JS, Waren M. Conduction in the right and left ventricle is differentially regulated by protein kinases and phosphatases: implications

for arrhythmogenesis. Am J Physiol Heart Circ Physiol. 2019;316:H1507–H1527. [PubMed: 30875259]

13. Benoist D, Dubes V, Roubertie F, Gilbert SH, Charron S, Constantin M, Elbes D, Vieillot D, Quesson B, Cochet H, et al. Proarrhythmic remodelling of the right ventricle in a porcine model of repaired tetralogy of Fallot. Heart. 2017;103:347–354. [PubMed: 28051771]
14. Morita H, Zipes DP, Lopshire J, Morita ST, Wu J. T wave alternans in an in vitro canine tissue model of Brugada syndrome. Am J Physiol Heart Circ Physiol. 2006;291:H421–8. [PubMed: 16648179]
15. Zhou P, Yang X, Li C, Gao Y, Hu D. J. Quinidine depresses the transmural electrical heterogeneity of transient outward potassium current of the right ventricular outflow tract free wall. J Cardiovasc Dis Res. 2010;1:12–8. [PubMed: 21188084]
16. Shivkumar K, Ardell JL. Cardiac autonomic control in health and disease. J Physiol. 2016;594:3851–2. [PubMed: 27417670]
17. Fukuda K, Kanazawa H, Aizawa Y, Ardell JL, Shivkumar K. Cardiac Innervation and Sudden Cardiac Death. Circ Res. 2015;116:2005–19. [PubMed: 26044253]
18. Machhada A, Marina N, Korsak A, Stuckey DJ, Lythgoe MF, Gourine AV. Origins of the vagal drive controlling left ventricular contractility. J Physiol. 2016;594:4017–30. [PubMed: 26940639]
19. Pauziene N, Alaburda P, Rysevaite-Kyguoliene K, Pauza AG, Inokaitis H, Masaityte A, Rudokaite G, Saburkina I, Plisiene J, Pauza DH. Innervation of the rabbit cardiac ventricles. J Anat. 2016;228:26–46. [PubMed: 26510903]
20. Ulphani JS, Cain JH, Inderyas F, Gordon D, Gikas PV, Shade G, Mayor D, Arora R, Kadish AH, Goldberger JJ. Quantitative analysis of parasympathetic innervation of the porcine heart. Heart Rhythm. 2010;7:1113–9. [PubMed: 20381645]
21. Jalife J. Ventricular Fibrillation: mechanisms of initiation and maintenance. Annu Rev Physiol. 2000;62:25–50. [PubMed: 10845083]
22. Tabereaux PB, Dosdall DJ, Ideker RE. Mechanisms of VF maintenance: Wandering wavelets, mother rotors, or foci. Heart Rhythm. 2009;6:405–15. [PubMed: 19251220]
23. Allessie MA, de Groot NM, Houben RP, Schotten U, Boersma E, Smeets JL, Crijns HJ. Electropathological substrate of long-standing persistent atrial fibrillation in patients with structural heart disease longitudinal dissociation. Circ Arrhythm Electrophysiol. 2010;3:606–15. [PubMed: 20719881]
24. Lou Q, Li W, Efimov IR. The role of dynamic instability and wavelength in arrhythmia maintenance as revealed by panoramic imaging with blebbistatin vs. 2,3-butanedione monoxime. Am J Physiol Heart Circ Physiol. 2012;302:H262–9. [PubMed: 22037192]
25. Aras KK, Faye NR, Cathey B, Efimov IR. Critical volume of human myocardium necessary to maintain ventricular fibrillation. Circ Arrhythm Electrophysiol. 2018;11:e006692. [PubMed: 30376733]
26. Noda T, Shimizu W, Taguchi A, Aiba T, Satomi K, Suyama K, Kurita T, Aihara N, Kamakura S. Malignant entity of idiopathic ventricular fibrillation and polymorphic ventricular tachycardia initiated by premature extrasystoles originating from the right ventricular outflow tract. J Am Coll Cardiol. 2005; 4;46:1288–94. [PubMed: 16198845]
27. Orozco-Duque A, Ugarte JP, Tobón C, Morillo C, Saiz J, Bustamante J. Dominant frequency, regularity and organization indexes response to preprocessing filter variations on simulated electrograms during atrial fibrillation. In: BIOSIGNALS 2013 - Proceedings of the International Conference on Bio-Inspired Systems and Signal Processing; 2013:306–309.
28. Gutbrod SR, Walton R, Gilbert S, Meillet V, Jaïs P, Hocini M, Haïssaguerre M, Dubois R, Bernus O, Efimov IR. Quantification of the transmural dynamics of atrial fibrillation by simultaneous endocardial and epicardial optical mapping in an acute sheep model. Circ Arrhythm Electrophysiol. 2015;8:456–465. [PubMed: 25713215]
29. Rogers JM, Usui M, Kenknight BH, Ideker RE, Smith WM. Recurrent Wavefront Morphologies: A Method for Quantifying the Complexity of Epicardial Activation Patterns. Ann Biomed Eng. 1997;25:761–8. [PubMed: 9300100]
30. Levandowsky M, Winter D. Distance between sets. Nature. 1971;234:34–35.

31. Tian L, Zimmerman B, Akhtar A, Yu KJ, Moore M, Wu J, Larsen RJ, Lee JW, Li J, Liu Y, et al. Large-area MRI-compatible epidermal electronic interfaces for prosthetic control and cognitive monitoring. Nat Biomed Eng. 2019;3:194–205. [PubMed: 30948811]
32. Insanally M, Trumpis M, Wang C, Chiang CH, Woods V, Palopoli-Trojani K, Bossi S, Froemke RC, Viventi J. A low-cost, multiplexed μeCoG system for high-density recordings in freely moving rodents. J Neural Eng. 2016;13:026030–26030. [PubMed: 26975462]
33. Coronel R, de Bakker JM, Wilms-Schopman FJ, Opthof T, Linnenbank AC, Belterman CN, Janse MJ. Monophasic action potentials and activation recovery intervals as measures of ventricular action potential duration: experimental evidence to resolve some controversies. Heart Rhythm. 2006;3:1043–50. [PubMed: 16945799]
34. Western D, Hanson B, Taggart P. Measurement bias in activation-recovery intervals from unipolar electrograms. Am J Physiol Heart Circ Physiol. 2015;308:H331–8. [PubMed: 25398981]
35. Streicher JM, Ren S, Herschman H, Wang Y. MAPK-Activated Protein Kinase-2 in cardiac hypertrophy and cyclooxygenase-2 regulation in heart. Circ Res. 2010;106(8):1434–43. [PubMed: 20339119]
36. Landstrom AP, Dobrev D, Wehrens XHT. Calcium Signaling and Cardiac Arrhythmias. Circ Res. 2017;120:1969–1993. [PubMed: 28596175]
37. Kong Q, Blanton RM. Protein Kinase G I and heart failure: shifting focus from vascular unloading to direct myocardial antiremodeling effects. Circ Heart Fail. 2013;6:1268–83. [PubMed: 24255056]
38. Gaborit N, Le Bouter S, Szuts V, Varro A, Escande D, Nattel S, Demolombe S. Regional and tissue specific transcript signatures of ion channel genes in the non-diseased human heart. J Physiol. 2007;582:675–693. [PubMed: 17478540]
39. Qin D, Singh JP. Low-Level Tragus Stimulation for Atrial Fibrillation: A Glimpse of Hope for Neuromodulation? JACC Clin Electrophysiol. 2020;6:292–294. [PubMed: 32192679]
40. Stavrakis S, Stoner JA, Humphrey MB, Morris L, Filiberti A, Reynolds JC, Elkholey K, Javed I, Twidale N, Riha P, et al. TREAT AF (Transcutaneous Electrical Vagus Nerve Stimulation to Suppress Atrial Fibrillation): A Randomized Clinical Trial. JACC Clin Electrophysiol. 2020;6:282–291. [PubMed: 32192678]
41. Stavrakis S, Humphrey MB, Scherlag BJ, Hu Y, Jackman WM, Nakagawa H, Lockwood D, Lazzara R, Po SS. Low-level transcutaneous electrical vagus nerve stimulation suppresses atrial fibrillation. J Am Coll of Cardiol. 2015;65:867–875. [PubMed: 25744003]
42. Yin J, Hu H, Li X, Xue M, Cheng W, Wang Y, Xuan Y, Li X, Yang N, Shi Y, et al. Inhibition of Notch signaling pathway attenuates sympathetic hyperinnervation together with the augmentation of M2 macrophages in rats post-myocardial infarction. Am J Physiol Cell Physiol. 2016;310:C41–53. [PubMed: 26491050]
43. Hadaya J, Ardell JL. Autonomic Modulation for Cardiovascular Disease. Front Physiol. 2020;11:617459. [PubMed: 33414727]
44. McGuirt AS, Schmacht DC, Ardell JL. Autonomic interactions for control of atrial rate are maintained after SA nodal parasympathectomy. Am J Physiol. 1997;272:H2525–33. [PubMed: 9227527]
45. Coote JH. Myths and realities of the cardiac vagus. J Physiology. 2013;591:4073–4085.
46. Rysevaite K, Saburkina I, Pauziene N, Vaitkevicius R, Noujaim SF, Jalife J, Pauza DH. Immunohistochemical characterization of the intrinsic cardiac neural plexus in whole-mount mouse heart preparations. Heart Rhythm. 2011;8:731–738. [PubMed: 21232628]
47. Nalliah CJ, Bell JR, Raaijmakers AJA, Waddell HM, Wells SP, Bernasochi GB, Montgomery MK, Binny S, Watts T, Joshi SB, et al. Epicardial Adipose Tissue Accumulation Confers Atrial Conduction Abnormality. J Am Coll Cardiol. 2020;76:1197–1211. [PubMed: 32883413]
48. Allessie MA, Boyden PA, Camm AJ, Kléber AG, Lab MJ, Legato MJ, Rosen MR, Schwartz PJ, Spooner PM, Van Wagoner DR, et al. Pathophysiology and prevention of atrial fibrillation. Circulation. 2001;103:769–777. [PubMed: 11156892]
49. Tabereaux PB, Walcott GP, Rogers JM, Kim J, Dosdall DJ, Robertson PG, Killingsworth CR, Smith WM, Ideker RE. Activation patterns of Purkinje fibers during long-duration ventricular

fibrillation in an isolated canine heart model. Circulation. 2007;116:1113–1119. [PubMed: 17698730]

50. Boukens BJ, Benjacholamas V, van Amersfoort S, Meijborg VM, Schumacher C, Jensen B, Haissaguerre M, Wilde A, Prechawat S, Huntrakul A, et al. Structurally abnormal myocardium underlies ventricular fibrillation storms in a patient diagnosed with the early repolarization pattern. JACC Clin Electrophysiol. 2020;6:1395–1404. [PubMed: 33121669]
51. Behr ER, Ben-Haim Y, Ackerman MJ, Krahnn AD, Wilde AAM. Brugada syndrome and reduced right ventricular outflow tract conduction reserve: a final common pathway? Eur Heart J. 2021;42:1073–1081. [PubMed: 33421051]

What is Known

- Right ventricular outflow tract (RVOT) is a common source of idiopathic ventricular arrhythmias (IVAs).
- However, the mechanisms underlying the RVOT's unique arrhythmia susceptibility remains not well elucidated due to lack of detailed electrophysiological and molecular studies of human RVOT.

What the Study Adds

- Human RVOT electrophysiology is characterized by shorter APD relative to the right ventricular apical region and drives the transmural dispersion of repolarization and transmural APD dispersion under normal physiological conditions.
- Cholinergic stimulation attenuates the arrhythmogenic effects of adrenergic stimulation, including increase in frequency of PVCs and shortening of wavelength.
- Arrhythmia in the RV is associated with weak positive spatio-temporal autocorrelation between the epicardial-endocardial arrhythmic wavefronts and reentrant rotors that are relatively more organized in the endocardium.

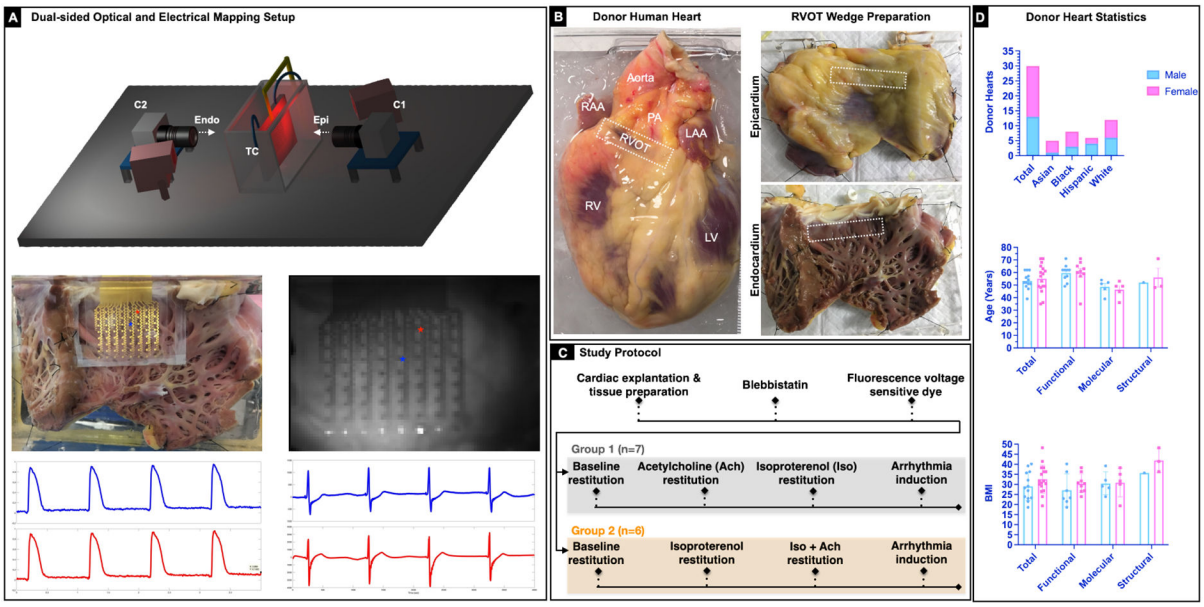

Figure 1. Experimental setup and study protocol

A: Schematic of the dual sided optical mapping setup (top). 64-electrode passive stretchable and translucent array to record electrical signals simultaneously with optical signals. Representative sample optical action potentials and electrograms from two locations on the endocardial surface are shown (bottom). **B:** Representative donor human heart and right ventricular outflow tract (RVOT) tissue wedge preparation. The RVOT region is identified on the epicardial and the endocardial surface (marked with a white dotted rectangle). **C**: Study protocol that includes Group 1 (N=7) and Group 2 (N=6) hearts. Group 1 experiments focused on evaluating the effects of sympathetic (isoproterenol 100nM) and parasympathetic stimulation (100 μM) in isolation. Group 2 experiments focused on evaluating the effect of parasympathetic stimulation post sympathetic stimulation. Arrhythmia induction was attempted in all hearts using S1S1 protocol and/or 50Hz burst pacing. **D:** Bar graph depicting break down of the 30 donor hearts by sex, age, BMI, and type of study.

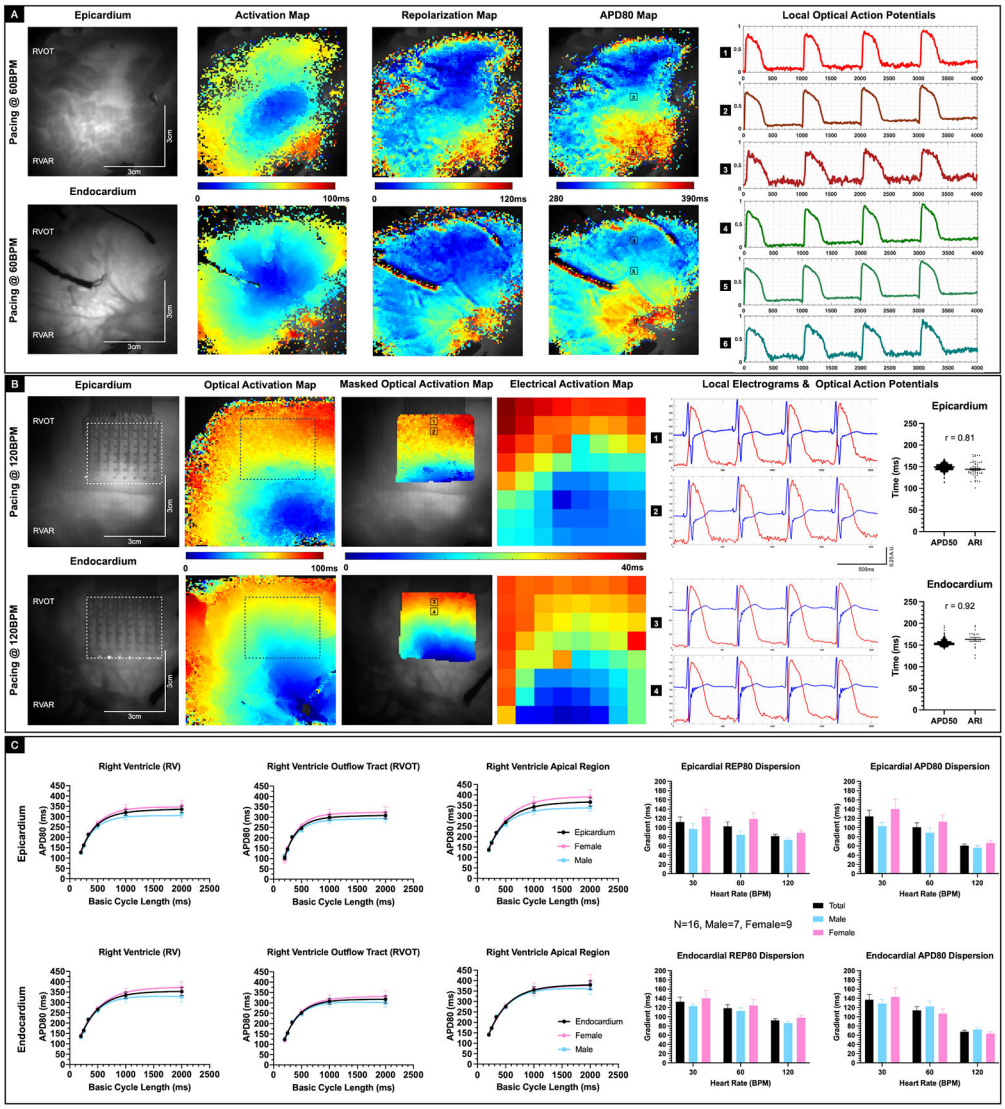

Figure 2. Baseline electrophysiology of donor human RVOT

A: Representative epicardial and endocardial activation, repolarization and action potential duration (APD80) maps from a Group 2 donor human heart (D11) paced at 60 BPM. Sample optical action potentials from the RVOT, RV mid wall, and RV apical region are also shown. **B:** Representative epicardial and endocardial activation maps from simultaneous optical and electrical recording in a Group 2 donor human heart (D14) paced at 120 BPM. Corresponding time aligned optical action potential and local electrograms from the RVOT region are also shown. Box plot shows correlation between APD50, and activation recovery interval (ARI) calculated from the local optical and electrical signals in the epicardial (R^2 = 0.65, Pearson's correlation) and endocardial region (R^2 = 0.84, Pearson's correlation). **C:** Baseline restitution curves from the RV, RVOT and RV apical epicardial and endocardial regions are shown (N=16, male=7, female=9). Female donor hearts trended to have relatively longer APD80 compared with male donor hearts, though not statistically significant. Representative epicardial and endocardial repolarization (REP80) and APD80

gradients at 30 BPM, 60 BPM, and 120 BPM are also shown. Females trended to have larger repolarization and APD80 gradients, but not statistically significant.

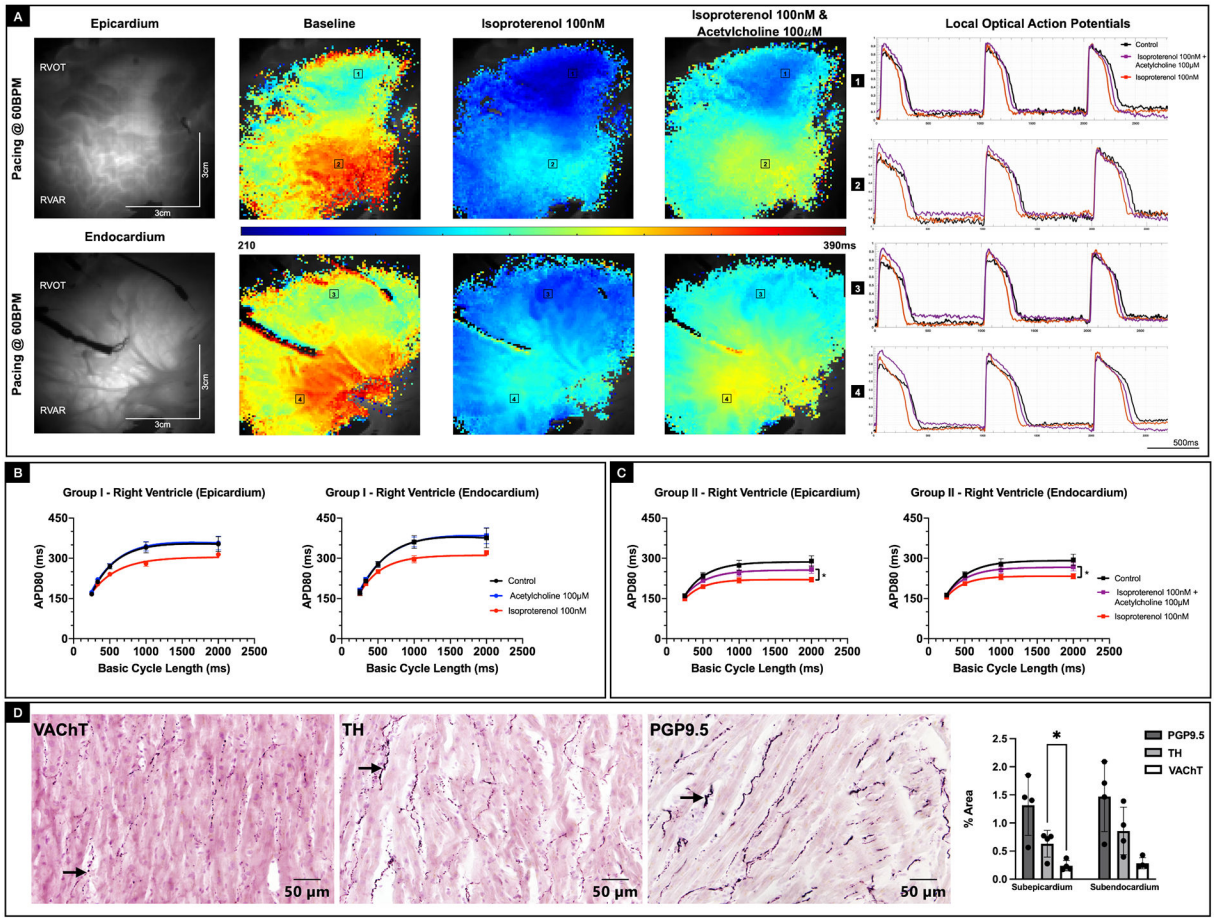

Figure 3: Effect of parasympathetic and sympathetic stimulation on APD80

A: Representative epicardial and endocardial APD80 maps from Group 2 donor human heart (D11) paced at 60BPM under baseline conditions, after treatment with isoproterenol (100nm) and finally after acetylcholine (100 μM) intervention in presence of isoproterenol. Corresponding optical action potentials from two locations in the RVOT and RV mid wall are also shown. **B:** Epicardial and endocardial APD80 restitution curves from Group 1 hearts, where the effects of sympathetic and parasympathetic stimulation were evaluated separately. While sympathetic stimulation shortened APD80, parasympathetic stimulation by itself had no effect on APD80. **C:** Epicardial and endocardial APD80 restitution curves from Group 2 hearts, where the effect of parasympathetic stimulation was evaluated in the presence of sympathetic stimulation. Acetylcholine attenuated the effects of isoproterenol with the recovery of APD80 trending towards baseline conditions ($p < 0.05$, Repeated measures 2-way ANOVA). **D:** Immunostaining of RVOT tissue sample from representative donor human heart (D28) shows the presence of VAChT-positive, PGP9.5-positive, and TH-positive nerve densities in both the sub-epicardial and the sub-endocardial regions.

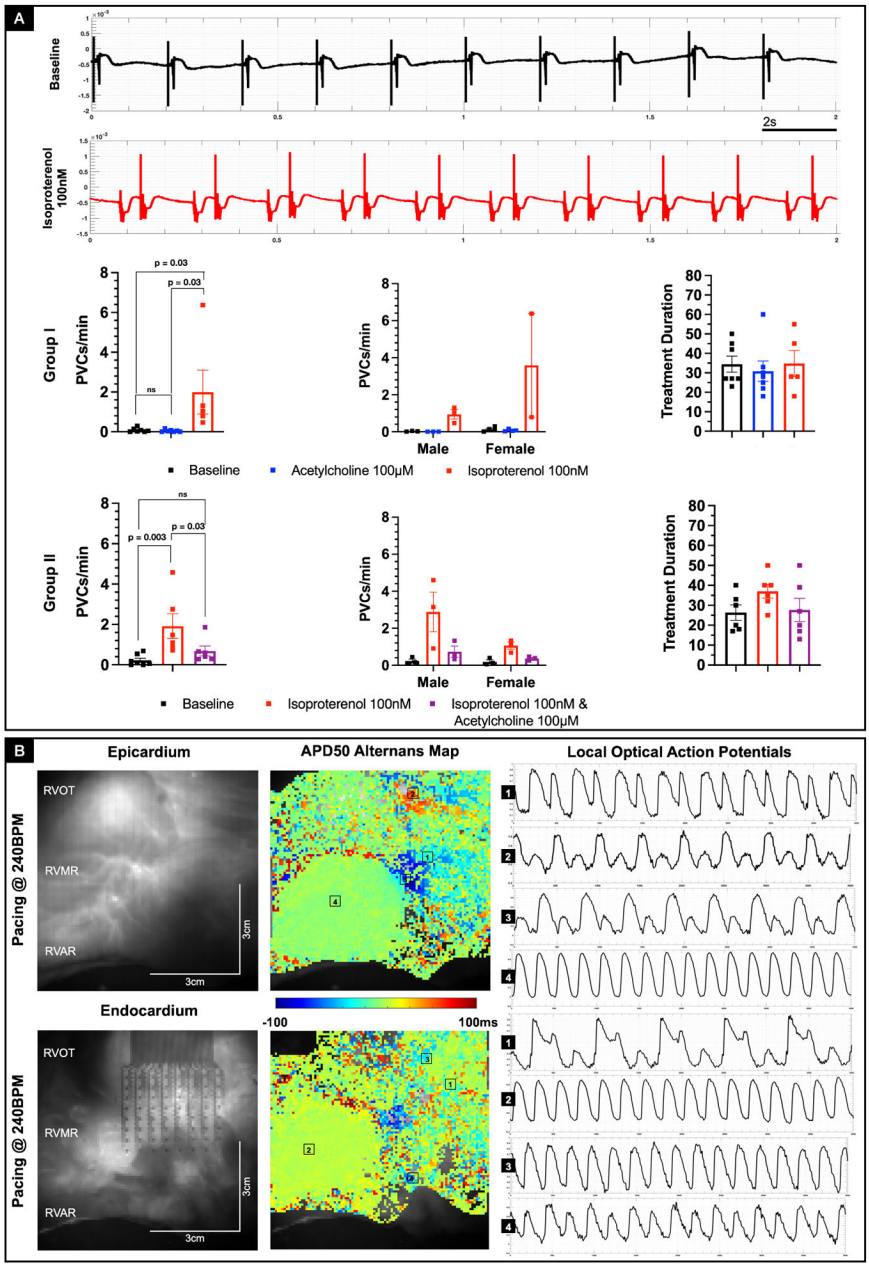

Figure 4: Effect of parasympathetic stimulation on arrhythmogenesis

A: Representative tissue chamber bath ECG recordings under baseline conditions and after treatment with isoproterenol 100nM from a representative Group 2 donor heart (D11). PVCs were observed after the intervention as shown. In Group 1 hearts, treatment with acetylcholine had no statistically significant effect on frequency of PVCs relative to baseline conditions, whereas treatment with isoproterenol increased the frequency of PVCs ($p = 0.035$, Ordinary ANOVA). In Group 2 hearts, acetylcholine intervention post treatment with isoproterenol decreased the frequency of PVCs ($p = 0.034$, Ordinary ANOVA). Sex related differences were not statistically significant. Treatment duration for each intervention across the two groups are also shown. **B:** Representative example of epicardial and endocardial

APD50 maps depicting discordant alternans in the RVOT as a consequence of S1S1 arrhythmia induction protocol in Group 1 donor human heart (D10). The alternans was triggered at the pacing rate of 240BPM. Corresponding sample optical action potentials from four different locations in the epicardial and endocardial regions are also shown.

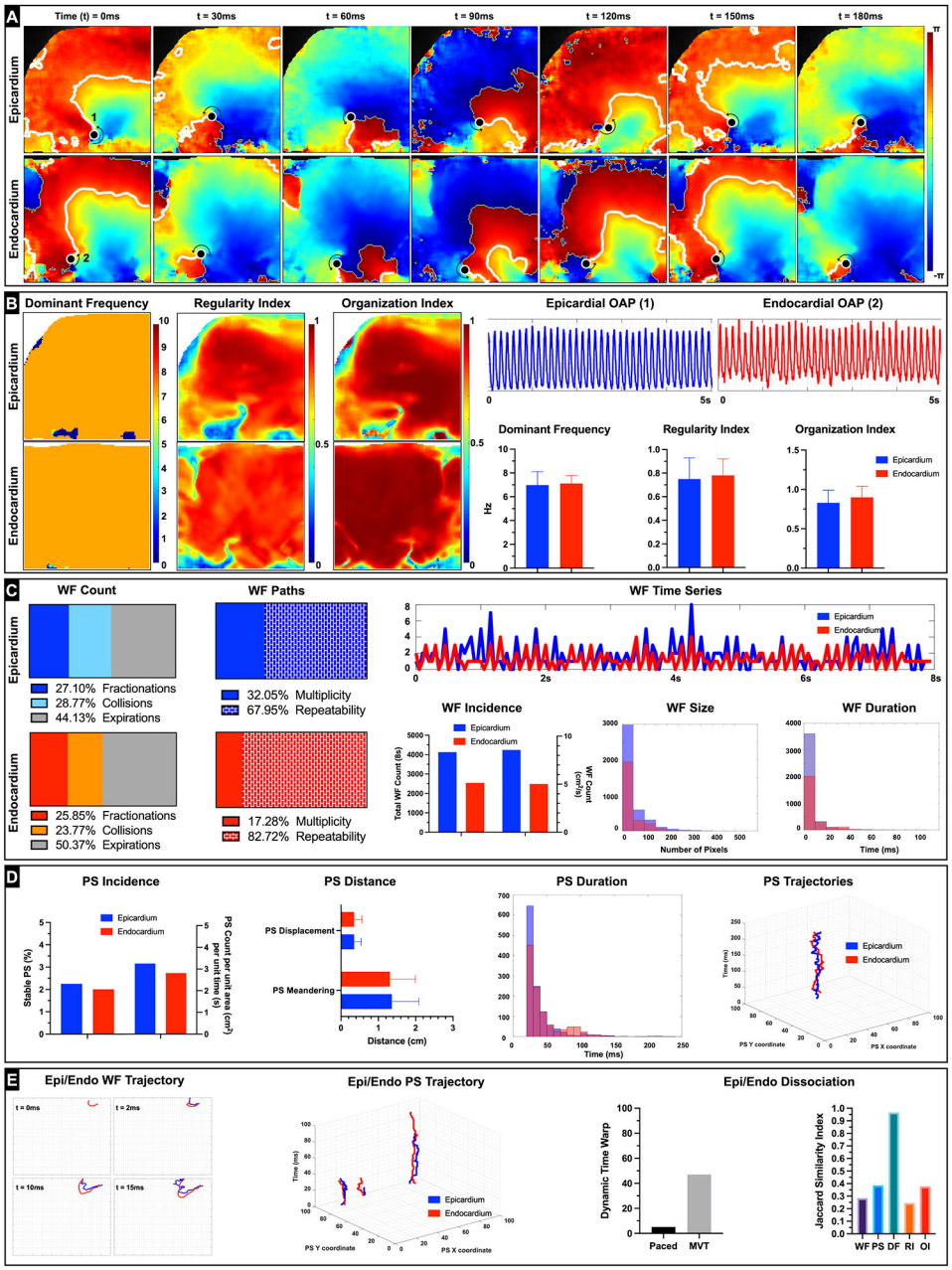

Figure 5: Monomorphic Ventricular Tachycardia (MMVT) dynamics

A: Representative epicardial and endocardial spatio-temporal phase maps depicting reentrant MMVT in donor human heart (D14) are shown. We can track the phase singularities (marked as a black dots) on both the epicardial and endocardial surfaces as the wavefronts complete one rotation (reentry) around the PS (rotor) over the duration of 180ms. **B:** Epicardial and endocardial DF, RI and OI maps along with the bar graphs are shown. Representative action potentials depicting MMVT from epicardial (1) and endocardial (2) locations are also shown. **C:** Wavefront dynamics including breakdown of epicardial and endocardial wavefronts by percentage of wavefronts that terminated in collisions, fractionations, or otherwise expired are shown. We also show percentage of

epicardial and endocardial wavefronts that were characterized as unique (multiplicity) or repeating (repeatability). Given that this arrhythmia exhibited MMVT characteristics, we see a relatively higher percentage of wavefront repeatability compared to other types of arrhythmias (e.g., VF). Epicardial and endocardial WF time series shows the relative congruence in the number of wavefronts incident on both surfaces at a given point of time. Dynamic time warp (DTW) was used to quantify the similarity between the two temporal sequences. Total number of wavefronts tracked over the duration of 8s as well as number of wavefronts per unit area (cm^2) and per unit time (s) are shown. We also show a histogram of wavefront size in pixels (1 pixel = approximately 0.07 cm) and a histogram of wavefront duration in milliseconds. **D:** Phase singularity (rotor) dynamics including total number of PS tracked over the duration of 8s as well as number of PS per unit area (cm^2) and per unit time (s) are shown. Bar graphs of PS displacement (minimum distance between starting location of the PS and location just prior to PS termination) and PS meandering (total path length traversed by the PS over its lifespan) along with a histogram of PS duration in milliseconds are shown. We also show a sample epicardial and endocardial PS trajectory. **E:** Epicardial and Endocardial dissociation dynamics included spatiotemporal autocorrelation analysis of wavefronts and PS. A representative example of epicardial and endocardial wavefront with similar trajectory over their first 15 ms is shown. Likewise, representative examples of three epicardial and endocardial PS with similar trajectories are also shown. Plot of the DTW values during pacing (120BPM) and during arrhythmia are shown. The relatively higher number denotes larger dissimilarity between the temporal sequences of epicardial and endocardial arrhythmic wavefronts in comparison to when the tissue was paced. Jaccard similarity index was used to quantify similarity between epicardial and endocardial wavefronts, phase singularities, DF, RI, and OI and is shown.

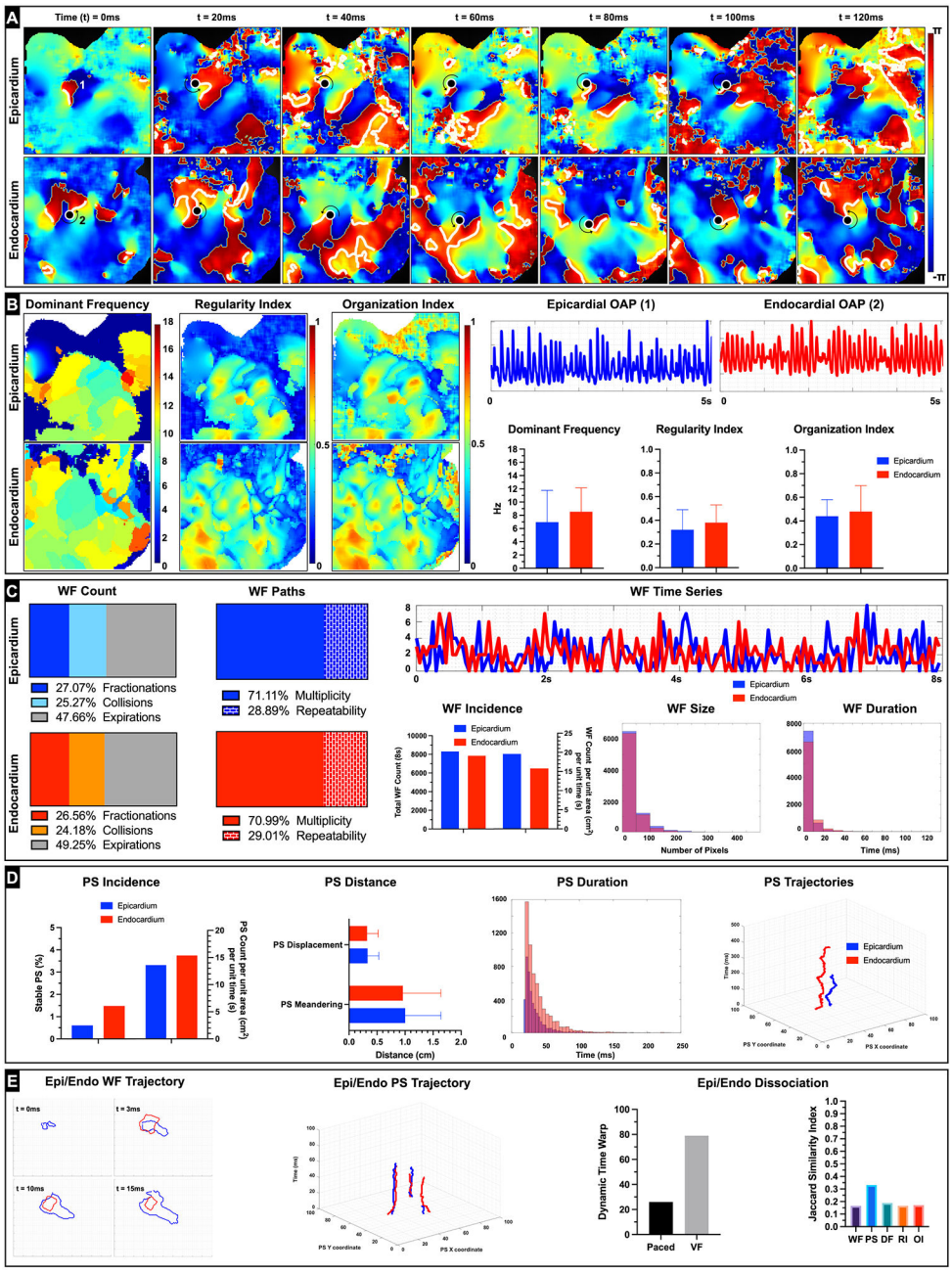

Figure 6: Ventricular Fibrillation (VF) dynamics

A: Representative epicardial and endocardial spatio-temporal phase maps depicting reentrant VF in donor human heart (D4) are shown. We can track the phase singularities (marked as a black dots) on both the epicardial and endocardial surfaces. In this instance we see the endocardial wavefront complete one rotation (reentry) around the PS (rotor) over the duration of 120ms. **B:** Epicardial and endocardial DF, RI and OI maps along with the bar graphs are shown and depict heterogeneity relative to that seen during MVT. Representative action potentials depicting VF from epicardial (1) and endocardial (2) locations are also shown. **C:** Wavefront dynamics including breakdown of epicardial and endocardial wavefronts by percentage of wavefronts that terminated in collisions, fractionations, or

otherwise expired are shown. We also show percentage of epicardial and endocardial wavefronts that were characterized as unique (multiplicity) or repeating (repeatability). Given that this arrhythmia exhibited VF characteristics, we see a relatively lower percentage of wavefront repeatability compared to other types of arrhythmias (e.g., MMVT). Epicardial and endocardial WF time series shows the relative congruence or lack thereof in the number of wavefronts incident on both surfaces at a given point of time. Dynamic time warp (DTW) was used to quantify the similarity between the two temporal sequences. Total number of wavefronts tracked over the duration of 8s as well as number of wavefronts per unit area (cm^2) and per unit time (s) are shown. We also show a histogram of wavefront size in pixels (1 pixel = approximately 0.07 cm) and a histogram of wavefront duration in milliseconds. **D:** Phase singularity (rotor) dynamics including total number of PS tracked over the duration of 8s as well as number of PS per unit area (cm^2) and per unit time (s) are shown. Bar graphs of PS displacement (minimum distance between starting location of the PS and location just prior to PS termination) and PS meandering (total path length traversed by the PS over its lifespan) along with a histogram of PS duration in milliseconds are shown. We also show a sample epicardial and endocardial PS trajectory. **E:** Epicardial and Endocardial dissociation dynamics included spatiotemporal autocorrelation analysis of wavefronts and PS. A representative example of epicardial and endocardial wavefront with similar trajectory over their first 15 ms is shown. Likewise, representative examples of three epicardial and endocardial PS with similar trajectories are also shown. Plot of the DTW values during pacing (120BPM) and during arrhythmia are shown. The relatively higher number denotes larger dissimilarity between the temporal sequences of epicardial and endocardial arrhythmic wavefronts in comparison to when the tissue was paced. Jaccard similarity index was used to quantify similarity between epicardial and endocardial wavefronts, phase singularities, DF, RI, and OI and is shown.

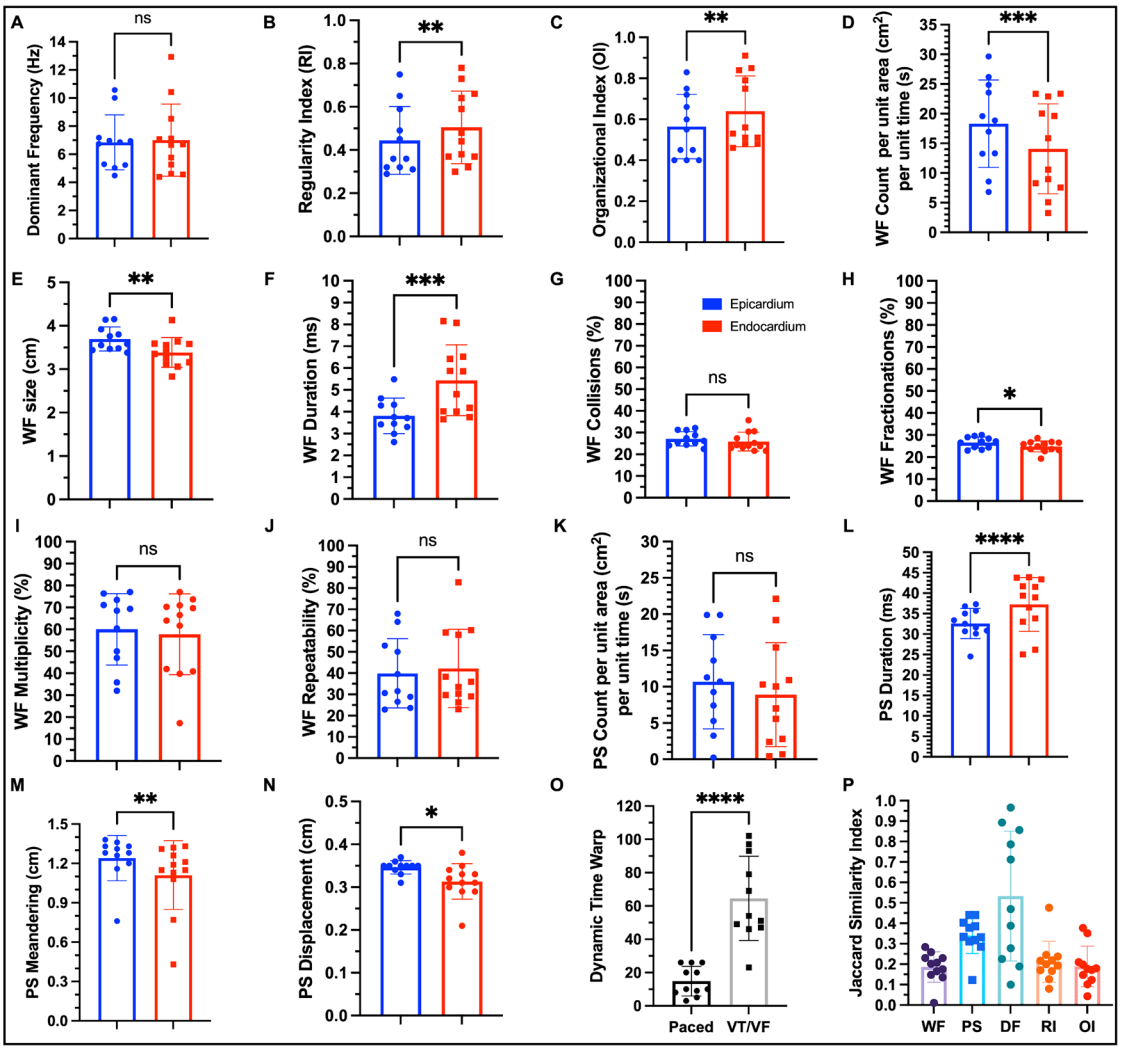

Figure 7: Statistical summary of arrhythmia dynamics

A: Dominant frequency was not statistically different between epicardium and endocardium. **B:** Regularity index was higher in the endocardium (p = 0.0026, paired t test). **C:** Organization index was higher in the endocardium (p = 0.0058, paired t test) suggesting that the arrhythmic wavefronts were more regular and organized in the endocardium in comparison with the epicardium. **D:** Number of wavefronts per unit area per unit time were higher in the epicardium (p = 0.0003, paired t test). **E:** Average size of the wavefronts was larger in the epicardium (p = 0.0034, paired t test). **F:** Average duration of the wavefronts was longer in the endocardium (p = 0.0001, paired t test). **G:** Percentage of wavefronts that terminated with collisions was not statistically different between the two surfaces. **H:** Percentage of wavefronts that terminated with fractionations (wavefront splitting into two or more wavefronts) was higher in the epicardium (p = 0.0174, paired t test). **I:** Percentage of wavefronts that were unique (multiplicity) was not statistically different between the two surfaces. **J:** Percentage of wavefronts that repeated their trajectories (repeatability) was not statistically different between the two surfaces. **K:** Number of PS per unit area per unit time was not statistically different between epicardium and endocardium. **L:** Average

duration of PS was longer in the endocardium in comparison with epicardium ($p < 0.0001$, paired t test). **M:** Average path length of the PS trajectory was longer in the epicardium ($p = 0.0093$, paired t test). **N:** Average distance traveled by the PS was smaller in the endocardium in comparison with epicardium ($p = 0.0286$, paired t test) suggesting that the PS was more spatially stable. **O:** The temporal sequences of arrhythmic wavefronts were more dissimilar than that of paced wavefronts as expected. **P:** There was weak positive spatio-temporal autocorrelation between epicardial and endocardial wavefronts and PS. Epicardial and endocardial local DF was more spatially correlated relative to local RI and local OI.

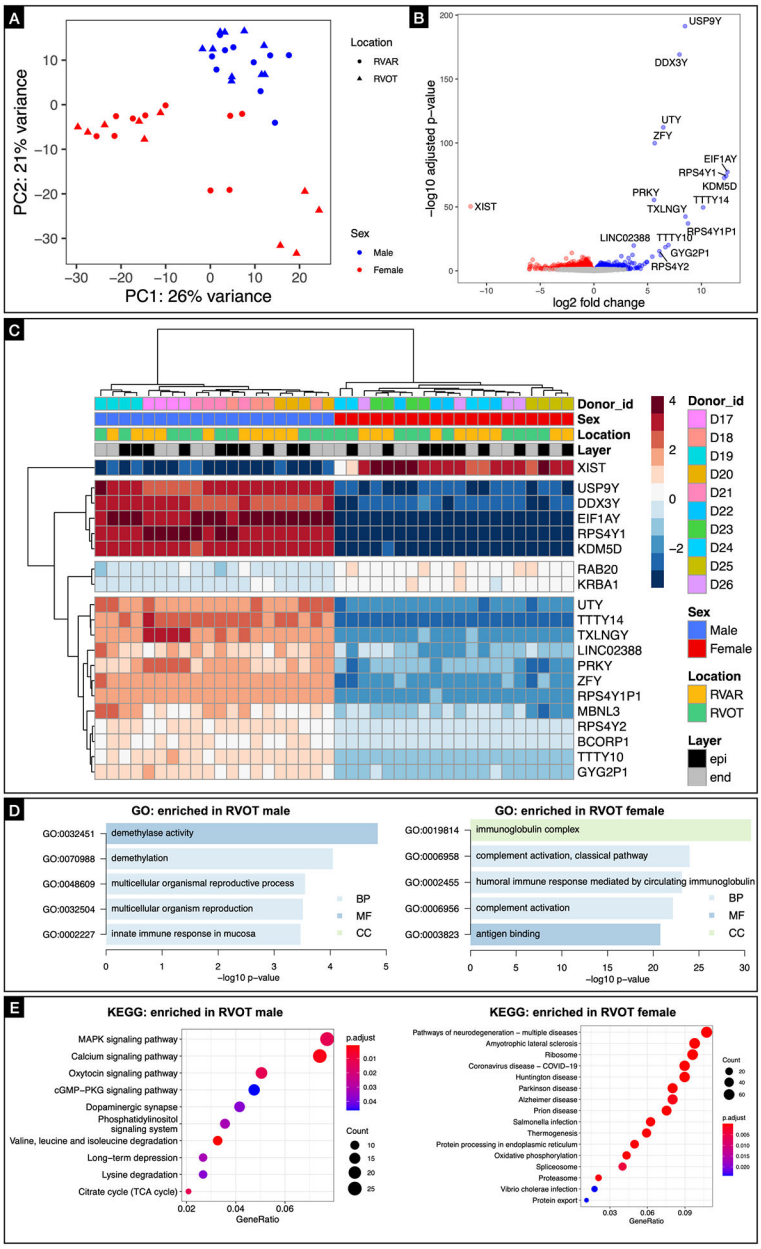

Figure 8: Transcriptome profiling of human RVOT

A: Principal component analyses showed that the tissue samples were clustered together by sex along the first principal component, which accounted for 26% of the observed variance. **B:** Volcano plot showing sex altered expression of 261 genes in the RVOT. **C:** Hierarchical clustering of both genes and the samples based on the gene expression profile (DEGs) in the gene expression matrix, identifying the top 20 genes. **D:** GO analysis suggest a trend that these sex-regulated genes are mainly involved in immunoglobin complex, humoral immune response etc., in case of females and demethylase activity, demethylation etc., in case of males. **E:** KEGG analysis revealed the top 16 KEGG-annotated pathways enriched for DEGs expressed in male and female RVOT.